

Laser-induced multiphoton dissociation branching ratios for H_2^+ and D_2^+

J. J. Hua and B. D. Esry

J. R. Macdonald Laboratory, Department of Physics, Kansas State University, Manhattan, Kansas 66506, USA

(Received 21 April 2009; published 23 July 2009)

The multiphoton dissociation branching ratios for H_2^+ and D_2^+ as a function of laser peak intensity and pulse length are investigated by solving the time-dependent Schrödinger equation in the Born-Oppenheimer approximation, neglecting nuclear rotation. An 800 nm laser pulse with peak intensities from 8×10^9 W/cm² to 10^{14} W/cm² and pulse lengths from 5 to 7.5 fs is used. We also investigate the viability of identifying zero-, one-, two-, and three-photon processes based only on the nuclear kinetic energy release spectrum, and check these identifications with a rigorous Floquet-like method.

DOI: [10.1103/PhysRevA.80.013413](https://doi.org/10.1103/PhysRevA.80.013413)

PACS number(s): 33.20.Xx, 33.80.Wz

I. INTRODUCTION

The rapid development of short pulse, intense-laser technology has given a strong boost to the study of molecular dynamics. Nowadays, the production of a femtosecond laser pulse, whose duration can be on the same time scale as the nuclear vibrational motion and whose field can be comparable with the internal Coulomb field of the molecule, has become routine. Several theoretical and experimental studies have shown that the interaction of molecules with ultrashort intense-laser pulses is sensitive to the characteristics of the laser pulse such as the peak intensity [1–3], pulse length [1,2], pulse shape [4,5], wavelength [6–11], and carrier-envelope phase [12–19].

The interaction between a molecule and an intense laser field can, in some ways, be thought of as a half collision. While this label is more appropriate to perturbative one-photon photodissociation, the same half-collision scattering states are used to analyze the molecular wave function following an intense-laser pulse. In contrast to the conventional full collision where there is incoming and outgoing flux, for a half collision, molecules are initially in bound rovibrational states and then dissociate or ionize due to the interaction with the laser field.

Many mechanisms have been invoked to interpret the breakup of molecules [7,9]. The most often mentioned are bond softening, vibrational trapping or bond hardening, above threshold dissociation (ATD) [20], below threshold dissociation [21], zero-photon dissociation [22], and charge-resonance enhanced ionization [23,24]. The latter is one of the main candidates for molecular ionization, also known as “Coulomb explosion” if the resulting nuclear fragments are fully stripped of electrons. Meanwhile, phenomena continue to be found in part through the application of technology. These phenomena include, for instance, above threshold Coulomb explosion [25] (see also [26]), which is ionization at laser intensities near the onset of ionization resulting in nuclear kinetic-energy spectra having peaks separated by the photon energy; high-order ATD, which is ATD from highly excited electronic states [1]; and ATD from vibrationally cold, ground state HD^+ ions formed in a linear electrostatic ion storage device [27].

In this paper, we will study the branching ratios for multiphoton dissociation of H_2^+ into p and H . Even though ATD

is now a common part of many researchers’ intuition, surprisingly little work has been devoted to calculating these branching ratios and quantifying the contributions of one-, two-, and three-photon processes to H_2^+ dissociation—especially for the short pulses now available. Miret-Artés *et al.* calculated branching ratios for a CW laser using a coupled-channel method combined with an artificial-channel technique for a wide range of intensities (from 10^8 to 10^{14} W/cm²) at 329.7 nm [28]. Yang and DiMauro calculated the branching ratios for various multiphoton processes as a function of intensity, but focused on the narrow range of intensities from 4×10^{12} to 10^{13} W/cm² at 532 nm for pulses longer than 100 fs [29]. More recently, Maruyama *et al.* studied the dissociation dynamics of H_2^+ in a 100 fs laser pulse at 800 and 1200 nm, with peak intensities ranging from 10^{12} – 10^{14} W/cm² using the quasistationary Floquet approach [30].

Although people question applying the notion of “photons” to few-cycle laser pulses, many still interpret the dynamics in terms of multiphoton transitions such as ATD. To investigate whether multiphoton processes can still be identified theoretically and experimentally in these short pulses, we calculate the nuclear kinetic-energy release (KER) spectra for H_2^+ and D_2^+ in 5–7.5 fs pulses. At the 800 nm wavelength we use, these are 2–3 cycle pulses and are shorter than the typical vibrational period of either species by roughly a factor of two. We extract the contributions of different multiphoton processes from the KER spectra using two different methods. The first is based solely on the KER; and the second, on the population of Floquet-like components in the wave function. Only the first method—or the equivalent time-of-flight spectrum—is, of course, available to experiment. We will compare these and discuss to what extent the KER alone can actually be used to determine the number of photons involved. It is important to note that the experimental arrangement we analyze is that of an H_2^+ beam target so that the initial nuclear wave packet is an *incoherent* sum over vibrational states [31] not the *coherent* wave packet appropriate to an experiment starting from neutral H_2 .

II. THEORETICAL BACKGROUND

We solve the time-dependent Schrödinger equation using two different methods. Both methods utilize the Born-

Oppenheimer approximation without nuclear rotation and fix the molecular axis along the linearly polarized laser field. The second method additionally expands the nuclear wave functions on photon states using a Floquet-like approach appropriate for laser pulses. Before giving the details specific to each method, we will discuss what is common to both.

We take the laser's electric field to be

$$\mathcal{E}(t) = \mathcal{E}_0(t)\cos(\omega t + \varphi), \quad (1)$$

where ω is the carrier frequency and φ is the carrier-envelope phase. The pulse envelope is $\mathcal{E}_0(t) = \mathcal{E}_0 e^{-(t/\tau)^2}$ with pulse length τ related to the FWHM of the intensity envelope by $\tau = \tau_{\text{FWHM}}/\sqrt{2 \ln 2}$. The amplitude of the electric field in atomic units is $\mathcal{E}_0 = \sqrt{I/3.51} \times 10^{16}$ W/cm² for a pulse with the peak intensity I in W/cm².

As mentioned above, the H₂⁺ was assumed to be produced in an ion source by electron impact ionization, which usually leads to a roughly Franck-Condon distribution of the vibrational states. The coherence of the vibrational states is assumed to be effectively lost due to the distribution of travel times of the molecular ions from the source to the reaction region since the distribution of travel times is much longer than the vibrational period [31]. Each vibrational state of each isotope is thus propagated independently, and the observables extracted in each case are incoherently summed with weights given by the Franck-Condon factors. We refer to these results as Franck-Condon averaged (FCA). To allow a more direct comparison with experiment, we also averaged over the laser's intensity distribution in the focal volume assuming the experimental geometry dictates integration only over the plane perpendicular to the laser propagation direction as is appropriate for recent experiments with H₂⁺ targets [31]. This intensity averaging thus requires the integration

$$\bar{P}(I_0) \propto \int_0^{I_0} \frac{P(I)dI}{I}, \quad (2)$$

for some physical observable $P(I)$ where I_0 is the peak laser intensity. Franck-Condon averaging enhances the contribution from the low-lying vibrational states, while intensity averaging emphasizes the low-intensity contribution.

We carried out calculations for an 800 nm laser pulse with peak intensities ranging from 8×10^9 W/cm² to 10^{14} W/cm² and pulse lengths from 5 to 7.5 fs. At the highest intensities, we tested the convergence with respect to the expansion on electronic states by including all of the states up to those converging to the $n=3$ manifold of H in the separated atom limit. It turned out, though, that all of the states in the $n=2$ and $n=3$ manifolds together contributed less than 1% to the total dissociation probability at 10^{14} W/cm². Consequently, we considered no intensities higher than this and included only the $n=1$ states, i.e., $1s\sigma_g$ and $2p\sigma_u$, in the results presented here. This simplification is consistent with our goal of determining whether KER alone is sufficient to identify the probability of different photon processes.

The observables that we focus on are the total dissociation probability and the KER spectrum. From these, we obtain the

multiphoton branching ratios. The total dissociation probability is calculated by projecting the time-dependent wave function on all of the bound states and subtracting the result from unity. The KER spectrum is calculated by projecting the time-dependent wave function onto energy-normalized nuclear continuum energy eigenstates.

A. Time-dependent Born-Oppenheimer

The details of our implementation of the time-dependent Born-Oppenheimer method for solving the time-dependent Schrödinger equation are given in Ref. [31]. Briefly, the electronic degrees of freedom were expanded on the field-free Born-Oppenheimer states, leaving coupled time-dependent equations in the internuclear distance R :

$$i \frac{\partial}{\partial t} \mathbf{F}(R, t) = \left[-\frac{1}{2\mu} \mathbf{I} \frac{\partial^2}{\partial R^2} + \mathbf{U}(R) - \mathcal{E}(t) \mathbf{D}(R) \right] \mathbf{F}(R, t). \quad (3)$$

The matrix \mathbf{I} is the unit matrix, $\mathbf{U}(R)$ is the diagonal matrix of Born-Oppenheimer potentials, μ is the nuclear reduced mass, and $\mathbf{F}(R, t)$ is the column vector containing the radial wave functions in each channel. The electronic dipole matrix elements $\mathbf{D}(R)$ have been evaluated in the length gauge as has been shown to be the only appropriate choice for a two-channel calculation [7]. Atomic units are used throughout this work unless otherwise specified. Equation (3) was solved using a split operator approximation to the short-time evolution operator, and the kinetic energy was approximated with a generalized three-point finite differences formula [32].

We used a nonuniform radial grid to improve efficiency and accuracy. In particular, more points were used at small R to represent both the rapid change in the wave function near the classical turning point and the shorter wavelengths present in the potential well. At large R , though, a linear grid—appropriate for nearly-free particles—was used, and slightly more than half of the points lie at $R \leq 20$ a.u. For a typical case it was verified that this nonuniform grid gives the same answer as a converged calculation with a uniform grid. To reduce reflection from the boundary at R_{max} , a sufficiently large grid was used, but no absorbing boundaries were applied. We used R_{max} up to 100 a.u., and the number of grid points is 3000–6000. The specific grid choices depend on laser peak intensity and pulse duration. A time step of 0.5 a.u. was sufficient to get 4–6 digit convergence in the total dissociation probability for the slow nuclear dynamics.

B. Time-dependent “Floquet”-Born-Oppenheimer

Since the number of photons exchanged with the laser field is not directly a physical observable, we wanted to try to find a definitive measure of this quantity. One natural approach is to utilize a Floquet method since it explicitly expands on photon channels. Normally, the Floquet representation is considered appropriate only for continuous wave (CW) lasers, although it has been adapted to treat pulses in a few cases [30,33]. We have recently derived, however, a particularly convenient Floquet-like representation of the time-dependent Schrödinger equation that is exact even for short pulses [18,34].

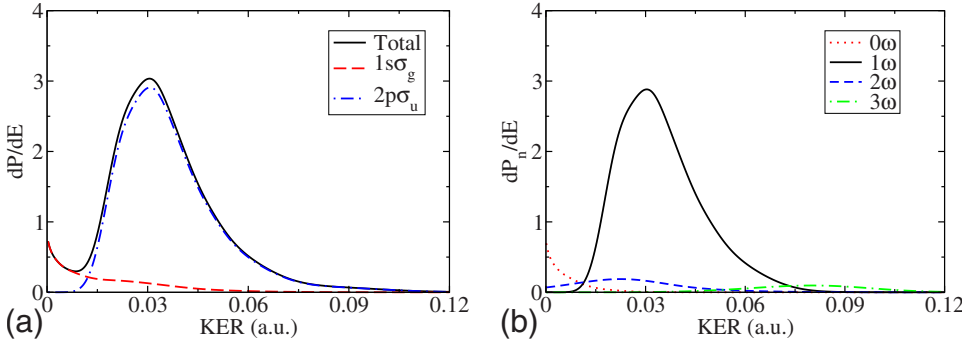


FIG. 1. (Color online) The Franck-Condon averaged nuclear kinetic energy release spectrum and the contributions from $1s\sigma_g$ and $2p\sigma_u$ for H_2^+ in an 800 nm, 5 fs laser pulse with peak intensity 5×10^{13} W/cm² from (a) Born-Oppenheimer and (b) Floquet-Born-Oppenheimer.

Our treatment takes advantage of the periodicity of Eq. (3) in φ to rewrite the nuclear-wave function $\mathbf{F}(R, t)$ using a discrete Fourier transform in φ [34]:

$$\mathbf{F}(R, t) = \sum_{n=-\infty}^{\infty} e^{in\varphi} e^{-in\omega t} \mathbf{G}_n(R, t). \quad (4)$$

Substituting this $\mathbf{F}(R, t)$ into (3) and equating the coefficients of the linearly independent functions $e^{in\varphi}$ gives

$$i \frac{\partial}{\partial t} \mathbf{G}_n = \left[\left(-\frac{1}{2\mu} \frac{\partial^2}{\partial R^2} - n\omega \right) \mathbf{I} + \mathbf{U} \right] \mathbf{G}_n - \frac{1}{2} \mathcal{E}_0(t) \mathbf{D}(\mathbf{G}_{n-1} + \mathbf{G}_{n+1}). \quad (5)$$

Any physical observable can be calculated just as for the time-dependent Born-Oppenheimer approach using Eq. (4).

We note that even though we do not invoke the Floquet theorem, our result, Eq. (5), closely resembles Floquet approaches [33]. This resemblance is clear and deliberate. The reason is that we want to tap into the intuition gained via the adiabatic Floquet picture [7,9] using the idea of photons (introduced here via the $e^{-in\omega t}$ factor). In fact, a little analysis shows that Eq. (5) can straightforwardly recover the Floquet equations in the CW limit, $\dot{\mathcal{E}}_0 = 0$. For these reasons and for simplicity, we will refer to our approach as “Floquet” or “Floquet-like” in our discussions as this emphasizes the connections rather than the differences.

In principle, we could have analyzed the nuclear wave functions from the solution of Eq. (3) using Eq. (4) to extract the functions $\mathbf{G}_n(R, t)$. It was more convenient, however, to simply solve Eq. (5) directly. We again used a split operator approximation with generalized finite differences for the kinetic energy operator, using the same radial grids as described in the previous section. At the highest intensities, 56 Floquet blocks distributed roughly symmetrically about the initial $n=0$ state were needed to get the total dissociation probability converged to four digits. Lower intensities did not require so many Floquet blocks. Care was taken to ensure that the Floquet results agreed with the time-dependent Born-Oppenheimer results: the total dissociation probability between the two methods agree to four digits at the highest intensity and to six digits at the lowest intensity.

III. ANALYSIS

Above threshold dissociation was so-named by analogy with above threshold ionization (ATI). In ATI, the photoelectron spectrum typically shows well-defined peaks separated by the photon energy. The peaks can thus be labeled by the number of photons absorbed by the electron with high confidence. Even though the nuclear KER spectrum for dissociation of H_2^+ hardly ever shows clearly separated peaks identifiable with a particular number of photons, different n -photon contributions are still often identified in spectra based on their KER only. As the pulse length gets shorter—and the bandwidth larger—both the ATI and ATD spectra increasingly lose whatever structure they do have, making an energy-based identification of photon number even more difficult. Figure 1 shows the KER spectrum for H_2^+ in a 5 fs, 800 nm, 5×10^{13} W/cm² laser pulse. It shows one broad peak that cannot obviously be connected to a specific number of photons. Defining the n -photon dissociation probabilities P_n in our nonperturbative calculations is thus the key problem to be solved.

In our Floquet-Born-Oppenheimer approach, the definition is straightforward: P_n is the dissociation probability for a given n -photon channel. The language of the Floquet representation can also be useful, however, for defining P_n from the solutions of Eq. (3). The diabatic Floquet potentials, which are the field-free Born-Oppenheimer potentials shifted by integer multiples of ω (in atomic units), are shown in Fig. 2. The diabatic potentials can be identified as the diagonal elements of the effective potential matrix in the Floquet-Born-Oppenheimer Eq. (5). Also sketched in Fig. 2 are the adiabatic Floquet potentials at a fixed field strength which are obtained from the diabatic potentials by diagonalizing the potential matrix including the dipole coupling due to the laser field. As discussed in Sec. II, only the lowest two Born-Oppenheimer potentials, $1s\sigma_g$ and $2p\sigma_u$, are shown since they are sufficient at the intensities considered here. The dynamics of the system can thus be understood in terms of the usual curve-crossing physics familiar from collisions studies.

Figure 2 helps us to quickly identify which KER one should expect for n -photon dissociation of a given vibrational level v since energy is approximately conserved in the plot [35]. All channels below the initial vibrational energy in the $1s\sigma_g - 0\omega$ curve are energetically accessible making them possible final states. For instance, vibrational states with energies near the crossing between $1s\sigma_g - 0\omega$ and $2p\sigma_u - 1\omega$ will dissociate primarily to $2p\sigma_u - 1\omega$ with a KER given by the

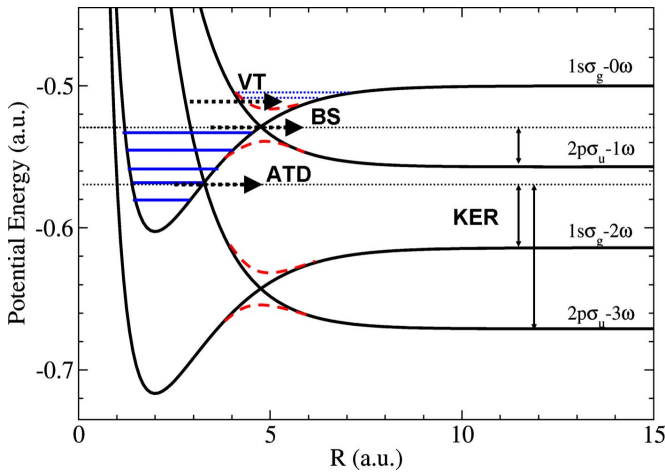


FIG. 2. (Color online) Diabatic Floquet potential curves for H_2^+ in a linearly polarized 800 nm intense laser field (thick solid lines). The adiabatic Floquet potentials are also sketched (thick dashed line). Different processes are indicated by dashed arrows: vibrational trapping (VT), bond-softening (BS), and above threshold dissociation (ATD). The horizontal dotted lines through the $1s\sigma_g-0\omega \rightarrow 2p\sigma_u-1\omega$ and $1s\sigma_g-0\omega \rightarrow 2p\sigma_u-3\omega$ crossings indicate typical dissociation energy. The KER expected in each case is also shown.

difference between the initial vibrational energy and the asymptotic $2p\sigma_u-1\omega$ threshold. This process is usually called bond softening. Those vibrational states lying between the $1s\sigma_g-0\omega \rightarrow 2p\sigma_u-1\omega$ and $1s\sigma_g-0\omega \rightarrow 2p\sigma_u-3\omega$ crossings will dissociate primarily to the $1s\sigma_g-2\omega$ and $2p\sigma_u-3\omega$ channels, resulting in ATD. Different initial vibrational states thus lead to different KER ranges for the same n -photon process.

If the laser were on continuously, energy would be strictly conserved in Fig. 2 [35]. Since we are treating a laser pulse, however, energy is only conserved to within roughly the bandwidth of the pulse. Consequently, vibrational states can dissociate to n -photon thresholds that lie energetically higher via processes generically labeled below threshold dissociation. One way to understand the mechanism producing below threshold dissociation is to imagine the adiabatic Floquet potentials varying in time according to the instantaneous value of $\mathcal{E}_0(t)$ [33]. In this picture, the gaps at the avoided crossings grow on the leading edge of the laser pulse and shrink on the trailing edge. For example, the potential well above the $1s\sigma_g-0\omega \rightarrow 2p\sigma_u-1\omega$ crossing can trap some part of the vibrational wave function on the leading edge of the pulse. As the intensity grows toward its maximum, the gap grows and the well is lifted. If the intensity is high enough, the well can disappear entirely, depositing anything trapped in it above the dissociation limit of the $1s\sigma_g-0\omega$ channel. This process is most efficient when the pulse is short so that the trapped wave function has insufficient time to dissociate to $2p\sigma_u-1\omega$ via nonadiabatic radial coupling. Below threshold dissociation thus becomes increasingly enhanced as the pulse length is shortened. When below threshold dissociation results in dissociation to the $1s\sigma_g-0\omega$ channel, it is labeled “zero-photon dissociation” [21]. This outcome is especially surprising since it represents dissociation with zero net photons absorbed [see, for example, Fig. 1(b)].

Since KER spectra like the one in Fig. 1—and similar experimental spectra—do not show a nice comb of peaks separated by ω , information in addition to the energy must be used to define P_n . Unfortunately, this information is only available to theory at this point. Our procedure consists of three basic steps: (i) use the dipole selection rules to associate even-number photon processes with $1s\sigma_g$ and odd-number processes with $2p\sigma_u$ and analyze them separately; (ii) analyze the spectra originating from different initial vibrational states separately; and (iii) apply energy criteria. We will refer to this procedure as the energy analysis method.

The dipole selection rules in our approximation just require that g states only couple to u states and vice versa. With an initial g state, the u state is populated only by odd numbers of photons. Similarly, starting from g , only even numbers of photons can lead to a final g state. If we analyze the KER spectrum for each molecular state separately, then any ATD peaks should be separated by 2ω , making them easier to identify. Figure 1 shows the $1s\sigma_g$ and $2p\sigma_u$ KER spectra in addition to the total. Unfortunately, they do not show substantially more structure than the total. The reason is that these spectra have already been averaged over the Franck-Condon distribution of vibrational states (as is appropriate for comparison with experiment).

To see separate peaks for different photon processes, we must look at the spectra for each initial vibrational state independently. Figure 3 shows the KER spectra in both the Born-Oppenheimer and Floquet-Born-Oppenheimer approaches for $v=3$ and 9, respectively, under the same conditions as Fig. 1. The $v=3$ state is the state nearest the $1s\sigma_g-0\omega \rightarrow 2p\sigma_u-3\omega$ crossing in Fig. 2, and $v=9$ is nearest the $1s\sigma_g-0\omega \rightarrow 2p\sigma_u-1\omega$ crossing. Even for this two-cycle laser pulse, the ATD structure is more clearly produced for each individual initial vibrational state than for the Franck-Condon-averaged total KER spectra. The different photon processes can thus be separated by energy if we analyze the KER spectra for each initial vibrational state independently, using the breakdown by molecular state. Note, however, that the 1ω KER spectrum from the Floquet-Born-Oppenheimer calculation in Fig. 3(d) shows two quite distinct peaks. Without the clear definition of P_n made possible by the Floquet approach, these would almost certainly be labeled different photon processes although they are separated by only about 0.6ω . More generally, the KER spectra for individual initial vibrational states at the highest intensities for these short pulses can still make identifying P_n based on energy a bit ambiguous. The Franck-Condon averaging will help improve the comparison between Born-Oppenheimer and Floquet-Born-Oppenheimer results.

The energies used to define different multiphoton processes are given in Tables I and II. As can be seen in the tables, it was not necessary to define unique ranges for each vibrational state. Rather, we could define energies appropriate for a group of states. To convince ourselves that the choices in the tables were not unreasonably sensitive to our definition, we varied the energy criteria by $\pm 5\%$ and checked the variation in the resulting P_n . If the relative change in P_n was less than $\pm 1\%$, the energy criteria were deemed acceptable.

Note that in our analysis we only consider zero- to three-photon processes because they account for more than 99% of

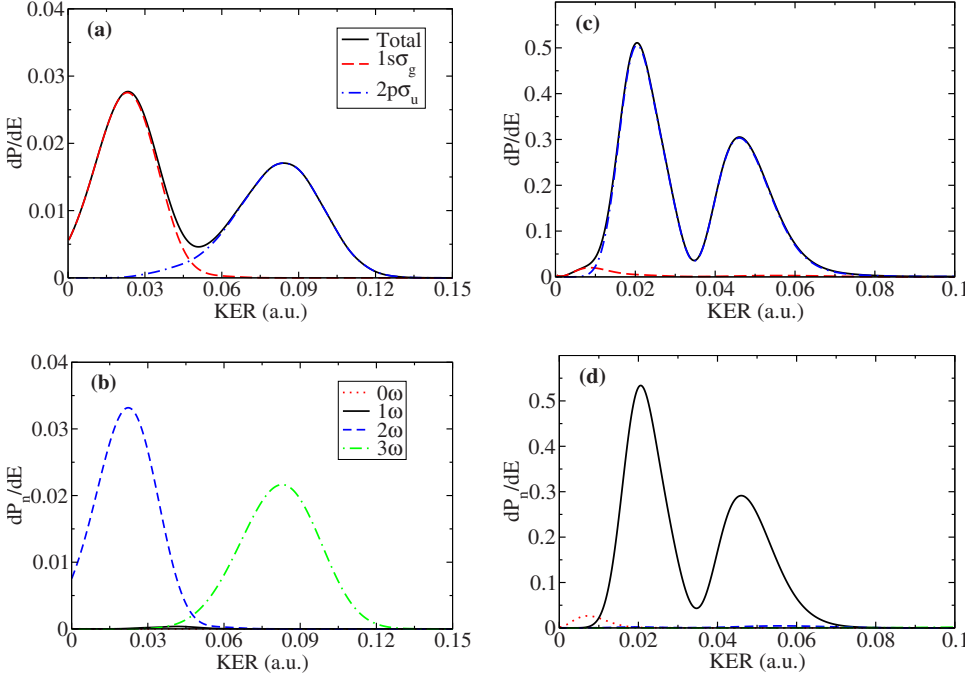


FIG. 3. (Color online) The nuclear kinetic-energy release spectrum for H_2^+ dissociation in an 800 nm, 5 fs laser pulse with peak intensity $5 \times 10^{13} \text{ W/cm}^2$. (a) and (b) are for an initial $v=3$ state; and (c) and (d), for $v=9$. In (a) and (c), the Born-Oppenheimer spectra are shown with the individual molecular state contributions; in (b) and (d), the Floquet-Born-Oppenheimer spectra for each photon channel are shown.

the total dissociation probability. While we do not calculate P_n for higher-order multiphoton processes, their effects are included in the time-dependent calculations. Except for the zero-photon dissociation channel, we do not separately identify below-threshold dissociation in our energy analysis either. Since below-threshold dissociation is initiated from more or less the same vibrational states as three-photon ATD and their energy spectra overlap in these few-cycle pulses, it is difficult to separate them. For example, vibrational states just below the $2p\sigma_u - 1\omega$ threshold, near the $1s\sigma_g - 0\omega \rightarrow 2p\sigma_u - 3\omega$ crossing, can dissociate to the $2p\sigma_u - 1\omega$ channel via below-threshold dissociation. Their contribution would tend to appear at low KER. The 1ω Floquet spectrum in Fig. 1(b) shows very little contribution at low KER, for instance, suggesting that below threshold dissociation is negligible for these pulse parameters. The lack of below threshold dissociation can also be seen in Fig. 3(b) where the one-photon

channel represents almost entirely below threshold dissociation. It peaks around 0.04 a.u., but can only be seen as a slightly thicker line for the figure frame (consistent with our assumption that it is negligible). This overlaps the lower edge of the three-photon ATD distribution and would thus be inseparable from it without the Floquet representation.

IV. RESULTS AND DISCUSSION

A. Comparison with “Floquet” approach

Before discussing the results of the calculations and analysis, we will show that the two methods for obtaining P_n discussed above do give agreement. More specifically, the less rigorous energy analysis method agrees with the Floquet approach. Since the Born-Oppenheimer calculations are much simpler—two channels rather than tens of channels for

TABLE I. Energy criteria used to define the multiphoton dissociation probabilities from the KER spectra for H_2^+ , grouped by initial vibrational state. All energies are in atomic units.

	$1s\sigma_g$	
	0ω	2ω
$v=0-8$	NA ^a	$0 \leq E \leq 0.0875$
$v=9-19$	$0 \leq E \leq 0.05$	$0.05 \leq E \leq 0.0875$
	$2p\sigma_u$	
	1ω	3ω
$v=0-4$	NA ^a	$0 \leq E \leq 0.116$
$v=5-8$	$0 \leq E \leq 0.105$	$0.105 \leq E \leq 0.116$
$v=9-19$	$0 \leq E \leq 0.105$	$0.105 \leq E \leq 0.116$

^aN/A.

TABLE II. Energy criteria used to define the multiphoton dissociation probabilities from the KER spectra for D_2^+ , grouped by initial vibrational state. All energies are in atomic units.

	$1s\sigma_g$	
	0ω	2ω
$v=0-11$	NA ^a	$0 \leq E \leq 0.0725$
$v=12-27$	$0 \leq E \leq 0.06$	$0.06 \leq E \leq 0.0725$
	$2p\sigma_u$	
	1ω	3ω
$v=0-5$	NA ^a	$0 \leq E \leq 0.15$
$v=6-11$	$0 \leq E \leq 0.12$	$0.12 \leq E \leq 0.15$
$v=12-27$	$0 \leq E \leq 0.12$	$0.12 \leq E \leq 0.15$

^aN/A.

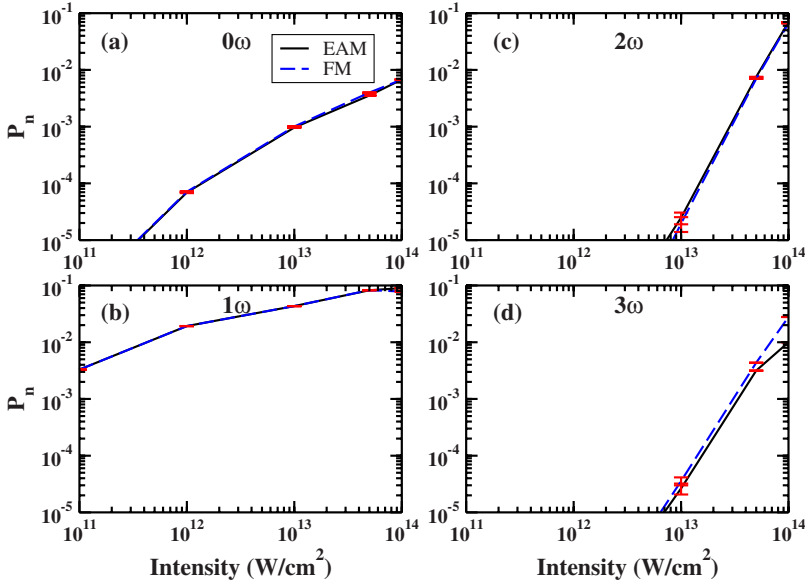


FIG. 4. (Color online) Comparison of Franck-Condon-averaged multiphoton dissociation probabilities P_n calculated by the energy analysis method (EAM) and the Floquet method (FM) for an 800 nm, 5 fs laser pulse. The error bars, shown in red, indicate the difference in the total dissociation probability from the two methods. Zero, one, two, and three photon dissociation probabilities are shown in (a),(b),(c), and (d), respectively.

Floquet-Born-Oppenheimer—this agreement reduces the computational burden significantly. All of the results in later sections will thus be based on the Born-Oppenheimer calculations combined with the energy analysis described in Sec. III.

Figure 4 compares the Franck-Condon averaged P_n from the two methods directly as a function of peak intensity for 5 fs, 800 nm laser pulses. Since these were obtained from two distinct calculations, there is some numerical error associated with each. We estimate this error from the difference in the total dissociation probabilities from the two methods and display it in the figure as the error bars shown for each P_n . Numerical convergence of the two calculations was separately checked with respect to the density of radial grid points, size of the radial grid, and the time step. As stated previously, the total dissociation probabilities thus obtained from the two methods agree to six digits at the lowest inten-

sity and four digits at the highest intensity. Consequently, only differences in P_n larger than these error bars should be regarded as arising from the energy analysis.

From Fig. 4, it can be seen that the agreement between the Floquet analysis and the energy analysis is best for the larger channels: 0ω and 1ω . The agreement for the weaker 2ω and 3ω channels is still quite good, and the agreement for all channels degrades with increasing intensity. Based on this agreement, we will only use the energy analysis to define P_n in the remainder of this work.

B. H_2^+

Figure 5 shows the multiphoton dissociation branching ratios as a function of laser pulse length for H_2^+ at two different laser peak intensities: 10^{13} W/cm² and 10^{14} W/cm². The branching ratios are defined as

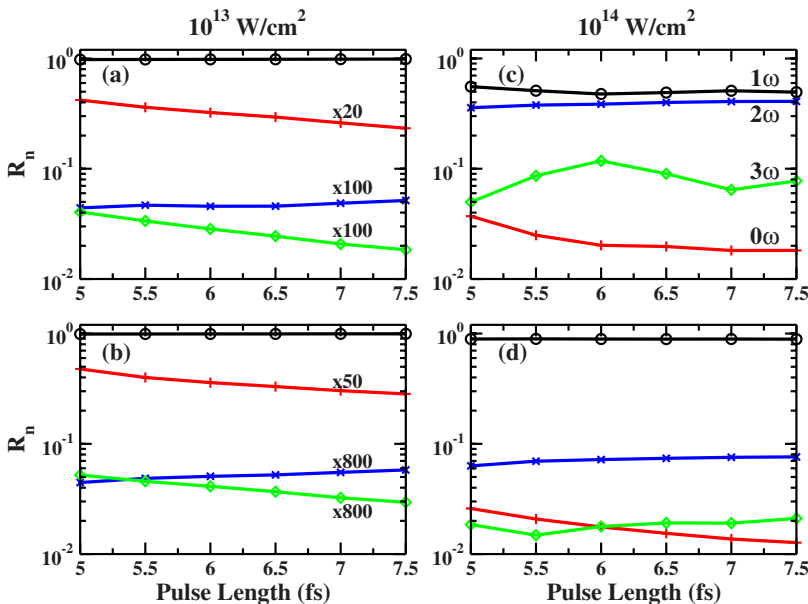
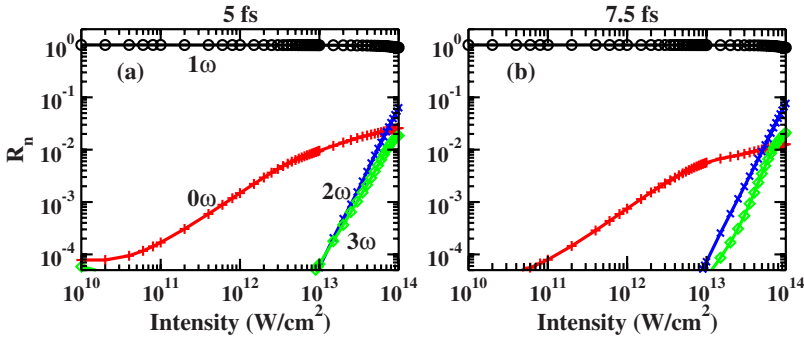


FIG. 5. (Color online) Multiphoton dissociation branching ratios R_n for H_2^+ at two different peak laser intensities: 10^{13} W/cm² (left column) and 10^{14} W/cm² (right column). (a) and (c) have been Franck-Condon averaged, while (b) and (d) are also intensity averaged. In the figure, zero, one, two, and three photon branching ratios are represented by red pluses, black circles, blue asterisks, and green diamonds, respectively.



$$R_n = \frac{P_n}{\sum_{n'} P_{n'}} \tag{6}$$

where R_n is the branching ratio for an n -photon process. The top row of the figure includes only Franck-Condon averaging, and the bottom row adds intensity averaging. Overall, the figure shows that multiphoton processes are more significant at higher intensity as expected.

Figure 5 shows that the 0ω and 3ω branching ratios trend generally downward with increasing pulse length, while the reverse is true for the 1ω and 2ω branching ratios. Since the mechanism for zero-photon dissociation can be thought of as nonadiabatic, it is suppressed as the pulse length grows. Conversely, the adiabatic pathways will grow more dominant in this limit, and the adiabatic pathways lead to the 1ω and 2ω channels. These trends are thus understandable qualitatively from the common picture of H_2^+ dissociation.

Quantitatively, the overwhelming dominance of the 1ω channel is expected, but the magnitude of the 0ω channel is not. Also a bit surprising is the fact that 0ω goes from the second largest channel to essentially the smallest channel when the intensity is changed from 10^{13} W/cm² to 10^{14} W/cm². Upon reflection, however, this intensity dependence can be understood by recognizing that the higher intensity pulse is effectively much longer since it spends a

longer time at and above the intensities important for vibrational trapping and thus zero-photon dissociation [22]. Longer pulses, of course, favor the adiabatic pathways over nonadiabatic ones, suppressing 0ω and 3ω as mentioned above. The suppression of the latter is also shown in the higher intensity results in the figure, supporting this interpretation.

The intensity-averaged results shown in the bottom row of Fig. 5 show that the 0ω channel is enhanced relative to the other channels. This is because intensity averaging emphasizes the contributions from lower intensities. Lower-order processes are thus enhanced by this averaging procedure. Using the perturbative result $P_n \propto I^n$, Fig. 4 shows that zero-photon dissociation is approximately a one-photon process. The 2ω channel, however, requires roughly four photons following the adiabatic pathway; and 3ω , three photons. The former sounds counterintuitive, but inspection of the Floquet potentials in Fig. 2 shows that a wavepacket must first exit the $1s\sigma_g-0\omega$ channel via a three-photon transition, then undergo an additional one-photon transition back to the $1s\sigma_g-2\omega$ channel—giving four photons in total. This dissociation pathway dominates direct two-photon transitions to $1s\sigma_g-2\omega$ since it is resonantly enhanced. The fact that the 2ω channel is actually higher-order than the 3ω is reflected in the relative enhancement of the 3ω channel in the intensity-averaged panels of Fig. 4.

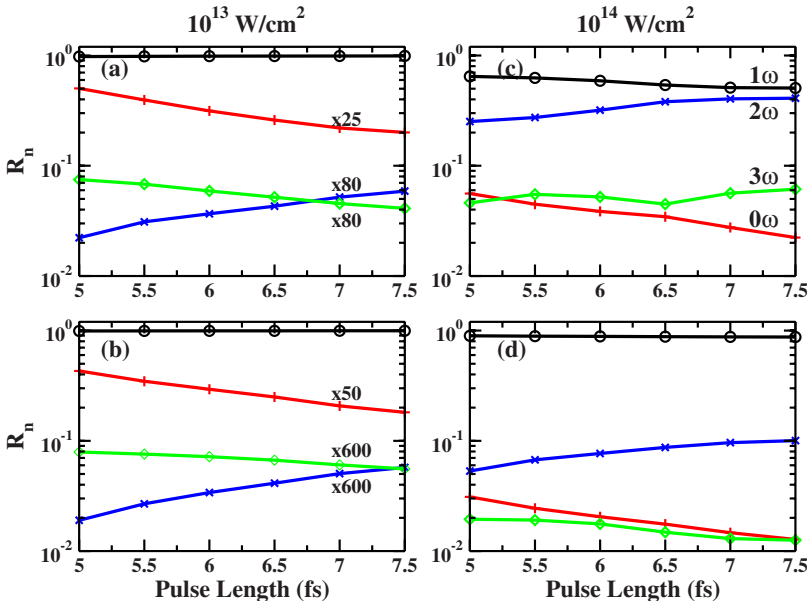


FIG. 7. (Color online) Multiphoton dissociation branching ratios R_n for D_2^+ at two different peak laser intensities: 10^{13} W/cm² (left column) and 10^{14} W/cm² (right column). (a) and (c) have been Franck-Condon averaged, while (b) and (d) are also intensity averaged. In the figure, zero, one, two and three photon branching ratios are represented by red pluses, black circles, blue asterisks, and green diamonds, respectively.

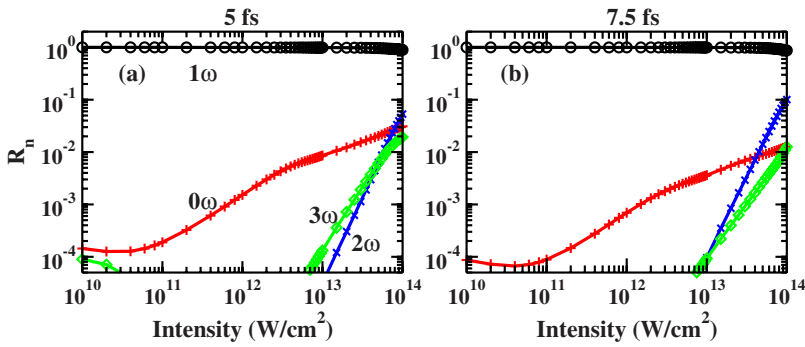


FIG. 8. (Color online) Multiphoton dissociation branching ratios R_n as a function of the laser peak intensity for D_2^+ in 800 nm, (a) 5 fs and (b) 7.5 fs laser pulses. In the figure, zero, one, two, and three photon branching ratios are represented by red pluses, black circles, blue asterisks, and green diamonds, respectively.

Taking another cut through parameter space, Fig. 6 shows the intensity dependence of the branching ratios for two different pulse lengths, including Franck-Condon and intensity averaging. As expected, the one-photon process is dominant at all intensities. The zero-photon process is larger than the two- and three-photon processes until about $7 \times 10^{13} \text{ W/cm}^2$, where the two-photon process takes the lead. The branching ratios for both pulse lengths behave essentially the same way as a function of intensity. The most substantial difference is the relative suppression of the 0ω channel in the longer pulse which was discussed above.

C. D_2^+

To check the effect of nuclear mass on the multiphoton branching ratios, we also calculated R_n for D_2^+ . Figure 7 shows R_n as a function of the pulse length using the same parameters as for D_2^+ and H_2^+ in Fig. 5. Any differences from H_2^+ can be assigned to the mass difference which leads to a slower D_2^+ wavepacket—or to an effectively shorter laser pulse [36]. Given the interpretations above based on adiabatic pathways and nonadiabatic transitions, we expect that D_2^+ will show differences from D_2^+ . Indeed, the 2ω channel is suppressed relative to H_2^+ . The pulse length at which the 3ω channel overtakes the nonadiabatic 0ω channel shifts to larger values for D_2^+ as well which is also consistent with F_2^+ experiencing an effectively shorter pulse. To complete the comparison, Fig. 8 shows the branching ratios as a function of intensity for D_2^+ .

V. SUMMARY

We have studied the multiphoton dissociation of H_2^+ and D_2^+ in an intense ultrashort laser pulse using the Born-Oppenheimer approximation. In particular, we focused on the branching ratios for different n -photon processes, trying to (i) establish a well-defined procedure for identifying them in the KER spectra, (ii) understand their systematic behavior for few-cycle pulses, and (iii) uncover the role of the mass in determining the probability of multiphoton transitions.

Since the intensities used in the calculations cover quite a wide range—from $8 \times 10^9 \text{ W/cm}^2$ to 10^{14} W/cm^2 —and the pulse lengths are short (from 5 fs up to 7.5 fs), this work extends previous studies of the branching ratios.

The behavior of the branching ratios can be understood by utilizing the standard picture of Floquet-Born-Oppenheimer potentials. The essential question to be answered is whether the system should follow the adiabatic pathway. To do so requires the laser pulse to be on when the wavepacket passes through each crossing. The adiabatic pathway is thus favored in longer pulses, and our calculations show that higher peak intensities are equivalent to longer pulses.

The issue of adiabaticity was also the determining factor in understanding the role of mass for these branching ratios. The heavier mass of the D_2^+ means that the nuclei move more slowly than for H_2^+ , pushing their behavior closer to the adiabatic limit in the same laser pulse.

Because the H_2^+ targets available currently have a wide range of vibrational states populated, it is essentially impossible to use only simple energy criteria to identify n -photon peaks in the total KER spectrum. By using additional information available in the calculations and comparing with a Floquet-like calculation, we validated a scheme appropriate to the commonly used two-channel Born-Oppenheimer approach. Until experiments can prepare H_2^+ targets in specific vibrational states, however, it is unlikely that a similar scheme can be applied experimentally.

ACKNOWLEDGMENTS

J.J.H. is grateful to Dr. J. McKenna for useful discussions and proofreading the manuscript. The authors thank Dr. J. V. Hernández for proofreading the manuscript. Sincere acknowledgment is given to all the members in Professor I. Ben-Itzhak's group for useful suggestions and discussions. This work was performed under auspices of the Chemical Sciences, Geosciences, and Biosciences Division, Office of Basic Energy Sciences, Office of Science, U.S. Department of Energy.

- [1] J. McKenna, A. M. Sayler, F. Anis, B. Gaire, Nora G. Johnson, E. Parke, J. J. Hua, H. Mashiko, C. M. Nakamura, E. Moon, Z. Chang, K. D. Carnes, B. D. Esry, and I. Ben-Itzhak, *Phys. Rev. Lett.* **100**, 133001 (2008).
- [2] J. T. Lin and T. F. Jiang, *Phys. Rev. A* **63**, 013408 (2000).
- [3] J. Ludwig, H. Rottke, and W. Sandner, *Phys. Rev. A* **56**, 2168 (1997).
- [4] K. C. Kulander, F. H. Mies, and K. J. Schafer, *Phys. Rev. A* **53**, 2562 (1996).
- [5] A. Rudenko, B. Feuerstein, K. Zrost, V. L. B. de Jesus, T. Ergler, C. Dimopoulou, C. D. Schröter, R. Moshhammer, and J. Ullrich, *J. Phys. B* **38**, 487 (2005).
- [6] A. Zavriyev, P. H. Bucksbaum, H. G. Muller, and D. W. Schumacher, *Phys. Rev. A* **42**, 5500 (1990).
- [7] A. Giusti-Suzor, F. H. Miest, L. F. DiMauro, E. Charron, and B. Yang, *J. Phys. B* **28**, 309 (1995).
- [8] K. Vijayalakshmi, A. Talebpour, T. T. Nguyen-Dang, J. Yang, A. D. Bandrauk, and S. L. Chin, *Phys. Rev. A* **62**, 053408 (2000).
- [9] J. H. Posthumus, *Rep. Prog. Phys.* **67**, 623 (2004).
- [10] A. S. Alnaser, M. Zamkov, X. M. Tong, C. M. Maharjan, P. Ranitovic, C. L. Cocke, and I. V. Litvinyuk, *Phys. Rev. A* **72**, 041402(R) (2005).
- [11] A. D. Bandrauk and H. Z. Lu, *Phys. Rev. A* **73**, 013412 (2006).
- [12] G. G. Paulus, F. Grasbon, H. Walther, P. Villorosi, M. Nisoli, S. Stagira, E. Priori, and S. De Silvestri, *Nature (London)* **414**, 182 (2001).
- [13] A. Gürtler, F. Robicheaux, W. J. van der Zande, and L. D. Noordam, *Phys. Rev. Lett.* **92**, 033002 (2004).
- [14] V. Roudnev, B. D. Esry, and I. Ben-Itzhak, *Phys. Rev. Lett.* **93**, 163601 (2004).
- [15] G. L. Kamta and A. D. Bandrauk, *Phys. Rev. Lett.* **94**, 203003 (2005).
- [16] Christian Per Juul Martiny and L. B. Madsen, *Phys. Rev. Lett.* **97**, 093001 (2006).
- [17] M. F. Kling, Ch. Siedschlag, A. J. Verhoef, J. I. Khan, M. Schultze, Th. Uphues, Y. Ni, M. Uiberacker, M. Drescher, F. Krausz, and M. J. J. Vrakking, *Science* **312**, 246 (2006).
- [18] V. Roudnev and B. D. Esry, *Phys. Rev. Lett.* **99**, 220406 (2007).
- [19] F. He and A. Becker, *J. Phys. B* **41**, 074017 (2008).
- [20] P. H. Bucksbaum, A. Zavriyev, H. G. Muller, and D. W. Schumacher, *Phys. Rev. Lett.* **64**, 1883 (1990).
- [21] L. J. Frasinski, J. H. Posthumus, J. Plumridge, K. Codling, P. F. Taday, and A. J. Langley, *Phys. Rev. Lett.* **83**, 3625 (1999).
- [22] L. J. Frasinski, J. Plumridge, J. H. Posthumus, K. Codling, P. F. Taday, E. J. Divall, and A. J. Langley, *Phys. Rev. Lett.* **86**, 2541 (2001).
- [23] T. Zuo and A. D. Bandrauk, *Phys. Rev. A* **52**, R2511 (1995).
- [24] T. Seideman, M. Y. Ivanov, and P. B. Corkum, *Phys. Rev. Lett.* **75**, 2819 (1995).
- [25] B. D. Esry, A. M. Sayler, P. Q. Wang, K. D. Carnes, and I. Ben-Itzhak, *Phys. Rev. Lett.* **97**, 013003 (2006).
- [26] A. Staudte, D. Pavicic, S. Chelkowski, D. Zeidler, M. Meckel, H. Niikura, M. Schoffler, S. Schossler, B. Ulrich, P. P. Rajeev, Th. Weber, T. Jahnke, D. M. Villeneuve, A. D. Bandrauk, C. L. Cocke, P. B. Corkum, and R. Dörner, *Phys. Rev. Lett.* **98**, 073003 (2007).
- [27] P. A. Orr, I. D. Williams, J. B. Greenwood, I. C. E. Turcu, W. A. Bryan, J. Pedregosa-Gutierrez, and C. W. Walter, *Phys. Rev. Lett.* **98**, 163001 (2007).
- [28] S. Miret-Artes, O. Atabek, and A. D. Bandrauk, *Phys. Rev. A* **45**, 8056 (1992).
- [29] B. Yang and L. F. DiMauro, *Laser Phys.* **3**, 398 (1993).
- [30] I. Maruyama, T. Sako, and K. Yamanouchi, *J. Phys. B* **37**, 3919 (2004).
- [31] P. Q. Wang, A. M. Sayler, K. D. Carnes, J. F. Xia, M. A. Smith, B. D. Esry, and I. Ben-Itzhak, *Phys. Rev. A* **74**, 043411 (2006).
- [32] M. W. J. Bromley and B. D. Esry, *Phys. Rev. A* **69**, 053620 (2004).
- [33] S.-I. Chu and D. A. Telnov, *Phys. Rep.* **390**, 1 (2004).
- [34] J. J. Hua and B. D. Esry, *J. Phys. B* **42**, 085601 (2009).
- [35] The “energy” in Fig. 2 is more properly thought of as a quasienergy in the sense of Floquet theory [33] since Eq. (5) reduces to the Floquet equations in the CW limit. The fact that one can treat energy as conserved in Fig. 2 is equivalent to the statement $E_i + n\omega = E_f$ where E_i is the initial energy, E_f is the final energy, and n is the net number of photons exchanged with the field.
- [36] J. J. Hua and B. D. Esry, *Phys. Rev. A* **78**, 055403 (2008).